ACS NANO
Cite This: ACS Nano XXXX, XXX, XXX−XXX
www.acsnano.org

ARTICLE

Transparent and Self-Powered Multistage Sensation Matrix for Mechanosensation Application

Qian Zhang,[†,‡,§] Tao Jiang,[†,‡] Donghae Ho,[∥] Shanshan Qin,[†,‡,§] Xixi Yang,[†,‡,§] Jeong Ho Cho,[∥,#] Qijun Sun,[*,†,‡] and Zhong Lin Wang[*,†,‡,⊥]

[†]Beijing Institute of Nanoenergy and Nanosystems, Chinese Academy of Sciences, Beijing 100083, China
[‡]National Center for Nanoscience and Technology (NCNST), Beijing 100190, China
[§]University of Chinese Academy of Sciences, Beijing 100049, China
[∥]SKKU Advanced Institute of Nanotechnology (SAINT) and [#]School of Chemical Engineering, Sungkyunkwan University, Suwon 440-746, South Korea
[⊥]School of Materials Science and Engineering, Georgia Institute of Technology, Atlanta, Georgia 30332-0245, United States

Supporting Information

ABSTRACT: **Electronic skin based on a multimodal sensing array is ready to detect various stimuli in different categories by utilizing highly sensitive materials, sophisticated geometry designs, and integration of multifunctional sensors. However, it is still difficult to distinguish multiple and complex mechanical stimuli in a local position by conventional multimodal E-skin, which is significantly important in the signals' feedback of robotic fine motions and human−machine interactions. Here, we present a transparent, flexible, and self-powered multistage sensation matrix based on piezoelectric nanogenerators constructed in a crossbar design. Each sensor cell in the matrix comprises a layer of piezoelectric polymer sandwiched between two graphene electrodes. The simple lamination design allows sequential multistage sensation in one sensing cell, including compressive/tensile strain and detaching/releasing area. Further structure engineering on PDMS substrate allows the sensor cell to be highly sensitive to the applied pressures, representing the minimum sensing pressure below 800 Pa. As the basic combinations of compressive/tensile strains or detaching/releasing represent individual output signals, the proposed multistage sensors are capable of decoding to distinguish external complex motions. The proposed self-powering multistage sensation matrix can be used universally as an autonomous invisible sensory system to detect complex motions of the human body in local position, which has promising potential in movement monitoring, human−computer interaction, humanoid robots, and E-skins.**

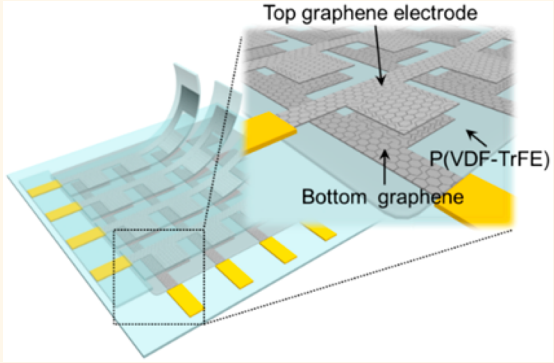

KEYWORDS: *electronic skin, multistage sensation, graphene, self-powering system, transparent*

With the rapid development of soft electronics, people look forward to developing a wearable system for measuring and quantifying physical signals generated by a human body to provide a facile route for physiological monitoring.[1−7] Electronic skin (E-skin) is a flexible circuitry matrix that is based on the mechanism of mechanosensation for mimicking the function of human skin to sense external stimuli, monitor human activity, and transduce external stimuli to electronic signals.[8−13] It has attracted significant research attentions toward highly sensitive materials, sophisticated geometry designs, facile manufacturing processes, and integration of multifunctional sensations.[14−18] To plausibly mimic human skin, various functional nanomaterials (nanowires, carbon nanotubes, and graphene) have been utilized as active materials for the sensation of different stimuli, such as pressure, temperature, humidity, and chemical/biomolecules.[8,12,19−23] Sophisticated geometrical design through an elaborate stack of different sensory films enables a highly integrated E-skin array capable of sensing multiple stimuli in one pixel.[8,23] In this way, a previously reported multimodal sensing array is ready to detect various stimuli in different categories. However, it is still difficult to distinguish

Received: August 29, 2017
Accepted: December 20, 2017
Published: December 20, 2017

DOI: 10.1021/acsnano.7b06126
ACS Nano XXXX, XXX, XXX−XXX

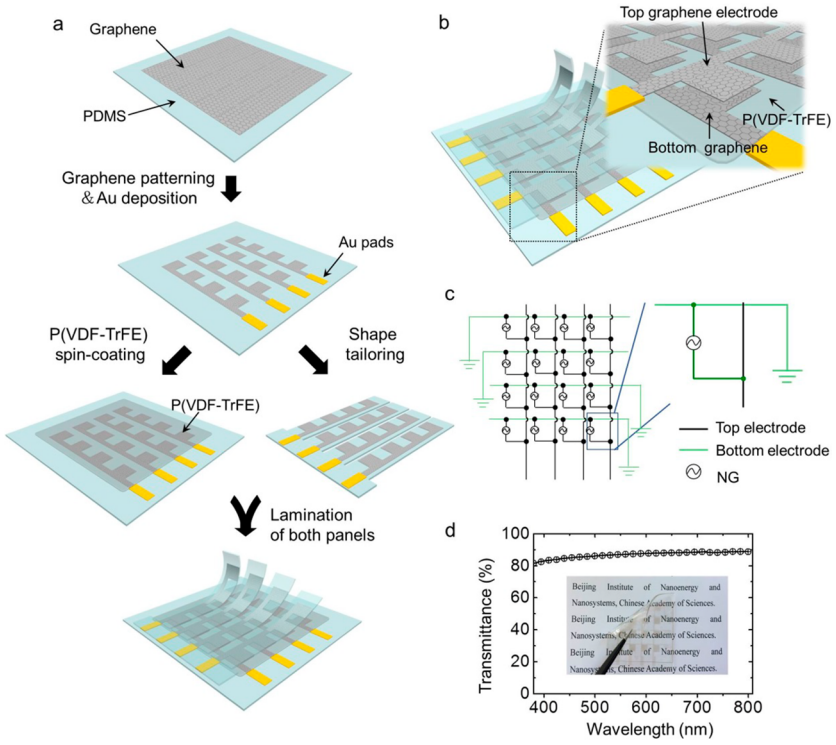

Figure 1. (a) Fabrication process of the self-powered multistage sensation matrix based on piezoelectric NGs. (b) Schematic illustration of the multistage sensation matrix. Inset shows the enlarged sensing pixel. (c) Circuit diagram of the sensation matrix. (d) Optical transmittance of the multistage sensation matrix fabricated on PDMS substrate. The inset shows the photographic image.

multiple and complex mechanical stimuli in a local position (*i.e.*, one pixel) by conventional multimodal E-skin, which is significantly important in the signals' feedback of robotic fine motions and human−machine interactions. Hence, it is necessary to develop a multistage sensation E-skin in rational device architecture.

Nanogenerators (NGs) have been extensively studied according to the great potential in harvesting mechanical energy, driving low-power personalized electronics, and constructing self-powered systems.[24−28] It is applicable to tactile sensors, touch pads, intelligent keyboards, and implanted devices.[29−33] These sensors can efficiently convert external mechanical stimuli into relevant electrical signals without input voltages, exhibiting excellent sensitivity, as well. As a wearable system, E-skin requires flexibility and transparency for conformal contact and visual imperception. The key challenge for a sensory matrix based on flexible nanogenerators is to select proper materials with good flexibility and mechanical stability paired with a facile fabrication process. Piezoelectric polymer with excellent flexibility, adequate mechanical strength, ease of processing, and chemical inertness is the primary choice as the active sensing materials. For transparent and flexible electrodes, graphene as a 2D hybridized carbon layer with outstanding electrical and mechanical properties has attracted great attention for applications in flexible electronics.[34−36] High-quality and large-area graphene are available as transparent conducting electrodes fabricated through chemical vapor deposition (CVD) and subsequent roll-to-roll transfer processes, exhibiting a sheet resistance as low as 125 $\Omega \cdot sq^{-1}$ with a 97% optical transmittance.[34] It is promising to use graphene and piezoelectric polymer for fabricating nanogenerators as a practical E-skin array.

In this paper, we present a transparent, flexible, and self-powered multistage sensation matrix based on piezoelectric NGs constructed in a crossbar design. Each sensor cell in the matrix comprises a layer of piezoelectric polymer sandwiched between two graphene electrodes. One of the graphene electrodes is patterned on polydimethylsiloxane (PDMS), whereas the other graphene electrode on the top layer of PDMS is laminated on the piezoelectric polymer. The simple lamination design allows sequential multistage sensation in one sensing cell, including compressive/tensile strain and detaching/releasing area. According to the piezoelectric potential induced by external strain and triboelectrification induced by detachment, the multistage sensation process is a self-powering behavior without any external voltage inputs. The nanogenerator cell demonstrates corresponding sensing relationships between output voltages and applied strains/detaching areas. The output signals induced by external compression/tension are related to the applied strains, while the sensing signals by the motion of detaching/releasing are mainly determined by the detaching areas and initial poling process. Further structure engineering on PDMS substrate allows the sensor cell to be highly sensitive to the applied pressures, representing the minimum sensing pressure below 800 Pa. Finally, the fabricated sensation matrix is demonstrated to detect the distribution of strains and detaching areas in two-dimensional color mapping. As the basic combinations of compressive/tensile strains or detaching/releasing represent individual output signals, the proposed multistage sensors are capable of decoding to distinguish external complex motions. The proposed self-powering multistage sensation matrix based on the laminated piezoelectric nanogenerator can be used universally as an autonomous invisible sensory system to detect complex motions of the human body in local position, which

DOI: 10.1021/acsnano.7b06126
ACS Nano XXXX, XXX, XXX−XXX

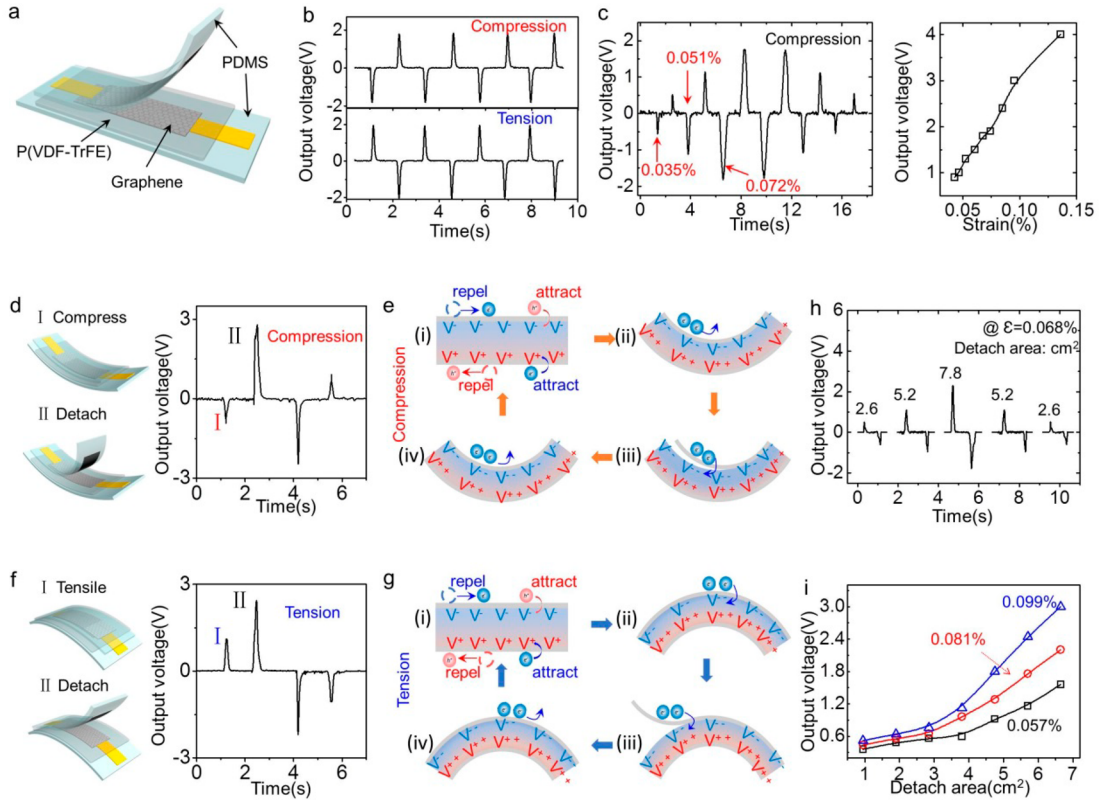

Figure 2. (a) Schematic illustration of the multistage sensor. (b) Piezoelectric sensing signals of the NG sensor under compressive (upper panel)/tensile (lower panel) strains. (c) Left panel shows the sensing signals of the strain sensor under different compressive strains (0.035, 0.051, 0.072, 0.072, 0.051, and 0.035%). The right panel shows the sensing output voltages *vs* applied strains. (d,f) Left panels are the schematic illustrations of the multistage sensation under compressive/tensile strains and subsequent detaching/releasing. The right panels display the corresponding sensing signals of the applied motion combinations. (e,g) Sensing mechanism under compressive/tensile strains, respectively. (h) Output signals according to different detachment areas under an applied strain at 0.068%. (i) Sensing output voltages *vs* the detached areas under different strains (0.057%, 0.081%, 0.099%).

has promising potential in movement monitoring, human–computer interaction, humanoid robots, and E-skins.

RESULTS AND DISCUSSION

Figure 1a illustrates the fabrication process of the self-powered multistage sensation matrix (4 × 4 strain sensors based on piezoelectric NGs). First, large-area graphene grown on a Cu foil was transferred onto the as-prepared PDMS thin film (6 × 6 cm^2) following the method in previous reports, which was depicted in the Methods section. The transferred graphene was patterned into four groups of electrodes with squared sensing pads by standard photolithography and reactive ion etching (RIE).[12] Au pads (30 nm) for electrical wiring were thermally deposited onto the ends of graphene electrodes. Then, poly(vinylidene fluoride-*co*-trifluoroethylene) (P(VDF-TrFE)) was spin-coated onto the PDMS–graphene substrate as the piezoelectric layer. Another PDMS panel with the same graphene electrode patterns was tailored into four-column shape and laminated onto the bottom PDMS substrate in a crisscross fashion to achieve the self-powered sensation matrix. Each sensing cell in the matrix comprises a P(VDF-TrFE) sensing layer sandwiched between two graphene electrodes (Figure 1b). When compressive/tensile stresses were applied to the NG sensing cell, different pulse voltage outputs correlated with external strains were produced according to the intrinsic piezoelectric properties of P(VDF-TrFE). In the same sensing cell, extra external motions of detaching/releasing the top graphene electrode could also be monitored due to the electrostatic balance. Thus, multistage sensation in a local position (including compressive/tensile strain and subsequent local detaching/releasing) in the matrix was achieved. Figure 1c shows the circuit diagram of the sensor array which is a typical passive matrix. P(VDF-TrFE) is utilized as the active sensing layer because P(VDF-TrFE) presents a stable piezoelectric crystalline β-phase at room temperature, promising a high output voltage. The copolymerization of PVDF and TrFE monomers leads to an all-trans conformation due to the addition of a third fluoride, which favors the formation of the piezoelectric β-phase.[37,38] As shown in Figure S1a, the intense and narrow (110/200) peak in the XRD spectra suggests a good crystallization of β-phase in the P(VDF-TrFE) after poling. The typical needle-like crystalline domains of the P(VDF-TrEF) was observed by scanning electron microscopy (Figure S1b). The sensor array also exhibits good optical transparency. Figure 1d and Figure S2 show the optical transmittance of the strain sensor array fabricated on a PDMS substrate, which reveals an overall transparency of 84% in the visible region, attributing to the excellent transparency of graphene electrodes and P(VDF-TrFE) layer.

Before characterization of the sensation matrix, the sensing properties of a single NG sensing cell were first tested. Figure 2a shows the device structure of the sensing cell. A graphene electrode on the top PDMS layer was laminated on the

DOI: 10.1021/acsnano.7b06126
ACS Nano XXXX, XXX, XXX–XXX

P(VDF-TrFE)/graphene/PDMS substrate. Typical piezoelectric performances (periodic pulse voltage outputs) were observed in Figure 2b. Due to the excellent piezoelectric properties of P(VDF-TrFE), opposite output voltages (−2 V/+2 V) were induced under compression/tension strains, respectively. As shown in the top panel of Figure 2b, a negative output voltage of −2 V was produced under a compressive strain of 0.098%, and an opposite voltage arose after releasing the strain. The operation mechanism of the piezoelectric nanogenerator is explained as depicted in Figure 2e,g. We took the compression case as an example and connected the bottom graphene electrode to be grounded. At the original state (Figure 2e(i)), electric dipoles were aligned downward in the P(VDF-TrFE) layer after the poling process. The negative dipole charge (V^-) repelled electrons and attracted holes at the top graphene electrode, while the positive dipole charge (V^+) repelled holes and attracted electrons at the bottom graphene electrode. Due to the large dielectric property of P(VDF-TrFE), the holes (electrons) accumulated at the interface region between the top (bottom) graphene sheet and P(VDF-TrFE), reaching electrostatic equilibrium. Under an external compressive strain (ii), the induced piezoelectric potential resulted in enhanced electric dipole charges (V^-/V^{++}). V^- drove the electron flow from the top graphene electrode to the bottom graphene electrode through an external load resistor, while V^{++} generated a flow of holes from the bottom graphene electrode to the top graphene, representing a negative output voltage. When the strain was released (i), the piezoelectric potential immediately vanished and the repelled electrons (holes) flowed back through the external circuit, giving rise to an opposite voltage pulse. In contrast, tensile strain led to an initial positive pulse output with subsequent negative pulse voltage after releasing (bottom panel of Figure 2b). The durability of the piezoelectric NG was tested over 800 bending−releasing cycles (Figure S3a), representing stable output performance for long-term usage.

To explore the sensing performances of the NG, the output signals of the sensor cell according to different applied strains were further characterized. The sensing cell was mounted on a bending system, and the compressive/tensile strains were applied by a step motor controller. By applying tensile strain onto the sensor cell (as illustrated in Figure S4), the strain in the length direction (ε_y) of the device is defined as $\varepsilon_y = h/2R$, where h is thickness of the device (135 μm, including the polymer substrate) and R is the bending radius. The left panel in Figure 2c shows the sensing signals of the strain sensor under different compressive strains (0.035, 0.051, 0.072, 0.072, 0.051, and 0.035%), and the corresponding output voltages are about 0.56, 1.13, 1.83, 1.83, 1.13, and 0.56 V, respectively. An approximately linear relationship between output voltages and applied strains was extracted, as shown in the right panel of Figure 2c. The output voltages increased from 1.5 to 4 V with the strains increasing from 0.06 to 0.14% due to the enhanced piezoelectric potentials. The linear curve is of great significance for sensing applications because of the excellent corresponding relations between output signals and external stimuli.

With top graphene electrode lamination on the P(VDF-TrFE) layer, local multistage sensation is available in a single sensing cell, including the compressive/tensile strains and subsequent detaching/releasing areas, as illustrated in the left panels of Figure 2d,f. Under a combination motion of compressive strain, detachment, release, and strain recovery, the corresponding output signals are shown in Figure 2d (right panel). The electrical signals I (−1 V) and II (2.8 V) in the right panel of Figure 2d were induced by the applied compressive strain (0.046%) and detachment (detaching electrode area is 7.5 cm^2), respectively. The equivalent output voltages in the opposite direction (−2.8 and 1 V) were observed after releasing the detached electrode and removing the strain, which was attributed to the flow back of the accumulated charges in the same amount.

The detailed working mechanism of multistage sensation is illustrated in Figure 2e, with the bottom graphene electrode grounded. When the device was subjected to a compressive strain, the top interface region repelled more electrons to the bottom interface region through the external circuit under the effect of enhanced dipole charges (ii), inducing a negative pulse output voltage. When the laminated top graphene electrode was detached from the P(VDF-TrFE) film, the accumulated holes at the top interface region were extricated from the electrostatic attractions by both piezoelectric dipoles and triboelectrification and flowed back from the top graphene electrode to the bottom electrode through the external circuit (iii), representing a positive pulse output voltage (2.8 V). Once the detachment was released, the piezopotential imposed the top interface region again and the holes flowed back from the bottom interface region, representing an opposite pulse output voltage (−2.8 V) equal to that induced by detachment (motion II). After the compressive strain was withdrawn, the piezoelectric potential vanished and the aligned dipoles recovered to their initial states. The repelled and attracted charges at both interface regions flowed back and yielded an output voltage at −1 V, opposite to that produced by applying compressive strain (motion I). Notably, the sensing signal induced by detaching/releasing (±2.8 V) was larger than that induced by applied strain/recovery (±1 V). This was because the sensing signal of detaching/releasing was measured without recovering the strain. The number of holes flowing back through the external circuit was contributed by both enhanced piezoelectric dipoles potential (applied strain) and triboelectrification (detachment). However, the sensing signal under applied strain (1 V) was only affected by the enhanced piezoelectric potential.

Similarly, output sensing signals under a combination motion of tensile strain, detachment, release, and strain recovery are shown in Figure 2f. The applied tensile strain (0.046%) and detaching area (7.5 cm^2) are the same with the compressive situation. Therefore, the positive pulse output voltage of 1 V induced by tension (Figure 2g) is in the same value but different directions compared with the output voltage induced by compression, which is in accordance with the typical output properties of piezoelectric NG (Figure 2b). The output voltage induced by detaching graphene electrode was 2.4 V at the same detaching area (7.5 cm^2) with the compressive situation. Notably, the output voltage originated from the detaching motion under tensile strain (2.4 V) was lower than that under the compressive strain (2.8 V). This was attributed to the extricated holes according to the detachment motion (which were extricated from the electrostatic attraction by the dipole charges) being partially neutralized by the attracted electrons induced by the applied tensile strain. After releasing the detachment and removing the tensile strain, both output signals in the negative directions (−2.4 and −1 V) were observed. The detailed working mechanism of the multistage sensation in the tensile case is illustrated in Figure 2f. The output signals induced by the detachments under both

DOI: 10.1021/acsnano.7b06126
ACS Nano XXXX, XXX, XXX−XXX

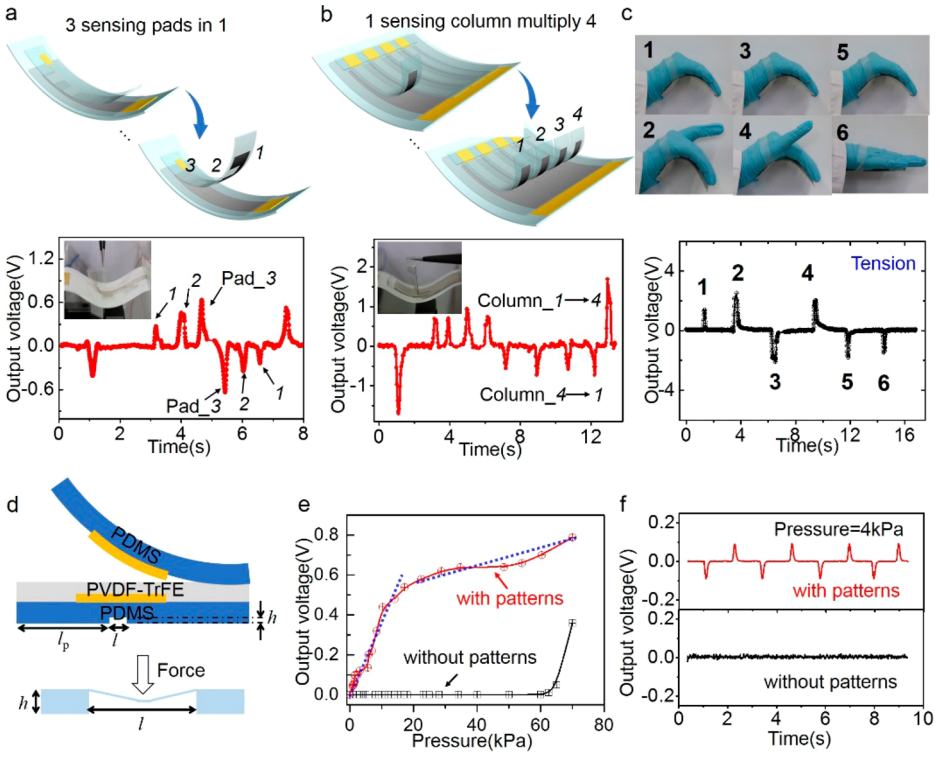

Figure 3. (a) Top graphene electrode was patterned into three pads (each pad area is 1 cm^2). The upper schematic illustration displays the pads detachment (from pad_1 to pad_3) under a compressive stain, and the corresponding sensing signals are shown in the bottom curve. (b) Top graphene electrodes were patterned into four columns (each column area is 3 cm^2) on the pretailored top PDMS layer. When the multiple sensing cell was subjected to compressive strain and manipulated with detachments in turn (from column_1 to column_4), the corresponding sensing signals were observed in the bottom panel. (c) Photo image of the four-column multiple sensor attached in the palm to capture the motion of hand bending and fingers lifting (top panel) and the corresponding sensing signals (bottom panel). (d) Cross section of the multistage sensor with groove pattern. (e) Output sensing voltages of the patterned and unpatterned sensing cells *vs* applied pressures. (f) Output sensing signals of patterned and untreated PDMS substrate under a pressure of 4 kPa.

compressive and tensile strains were positive (left panel of Figure 2d,f), mainly related to the accumulated charges at the top interface region in the electrostatic balance state after electrical poling. From the results obtained above, the output signals induced by external compression/tension are related with the applied strains, while the sensing signals by the motion of detaching/releasing are mainly determined by the detaching areas and initial poling process. Regardless the strain signals are in negative or positive direction under compression or tension, the signals induced by detachment maintain the positive direction. Meanwhile, the amplitudes of the detachment signals are inter-related to previous compression/tension signals. To confirm the coupling effect of piezoelectric potential and triboelectrification in the sensation of detaching/releasing motions, we conducted relevant experiments and theoretical simulations. First, we measured the output signals of the device under the motion of detaching/releasing without applying any strains to exclude the effect of piezoelectric potential. Typical pulse output signals were observed according to the contact electrification and electrostatic induction (*i.e.*, triboelectrification) between graphene and P(VDF-TrFE) (Figure S5a). Next, we applied strains and detaching/releasing motions to the multistage sensation device with polarized and unpolarized P(VDF-TrFE), respectively. The sensing signal of the detaching/releasing motion was greatly increased due to the enhanced surface charge density of the polarized P(VDF-TrFE) thin film.[39] To further verify the coupling effect between piezoelectric potential and triboelectrification, we simulated the potential distributions of multistage sensor by finite element method using COMSOL Multiphysics software (Figure S5c). The electrostatic potentials was enhanced/weaken under applied compressive/tensile strains, which was consistent with the experiment results, as shown in Figure 2d,f. Durability tests of bending/detachment motions for more than hundreds of cycles were also conducted. As shown in Figure S3b, the multistage sensor exhibits stable output signals after the external stimuli applied at different cycles (0, 200, and 400 cycles). In the durability test, one of main problems was the mechanical stability of the graphene electrodes during multiple detachment motions. In this work, the applied maximum bending strain was 0.1% in the length direction (ε_y), while the equivalent bending strain of the detachment was smaller than 0.5%, which is fully within the resistance recovery region (2%) and far less than the mechanical fracture strain (7%) of graphene.[40] The resistance of graphene electrode grown by CVD is able to be perfectly recovered under the applied strain below 2%, which is critical in the self-powered sensing behavior based on nanogenerators in order to maintain the internal resistance.

Figure 2h shows the output signals according to different detachment areas under an applied compressive strain at 0.068%. As the detached area increased from 2.6 to 7.8 cm^2, more charges were extricated from the restriction of electrostatic attraction, and the output voltage increased from 0.52 to 2.32 V, indicating the NG sensing cell can detect the detachment areas under certain strain. To further identify

DOI: 10.1021/acsnano.7b06126
ACS Nano XXXX, XXX, XXX−XXX

the sensing properties of the detachment areas related with the applied strains, Figure 2i demonstrates the sensing output voltages *versus* the detached areas under different strains (0.057%, 0.081%, 0.099%). Higher strain led to larger variation of sensing output voltages (equivalent to the sensitivity) under the same detachment areas, reaching the highest output voltage of 3 V with detaching area and applied strain at 6.65 cm^2 and 0.099%, respectively. This was consistent with the COMSOL simulation result and verified the coupling effect between piezoelectric potential and triboelectrification in the multistage sensation process. When higher external strain was applied to the multistage sensor, the enhanced piezoelectric dipoles electrostatically attracted more charges. Even if the laminated graphene was detached at the same area, more charges flowed back in the case of subjecting it to a higher applied strain according to the triboelectrification effect, exhibiting a larger sensing voltage at higher applied strain as shown in Figure 2i.

According to the lamination design, the structure of the NG sensor can be further engineered to realize sophisticated multistage sensation. Top graphene electrodes can be patterned into different shapes for diverse sensation functions. The bottom PDMS substrate can also be patterned to achieve higher sensitivity. As shown in the top panel of Figure 3a, the graphene electrode was patterned into three sensing pads (the area of each pad is 1 cm^2) in one graphene electrode. According to the facile detachment of the laminated graphene electrode, the patterned graphene pads can be detached one after another for stepped detachment sensation. The bottom curve of Figure 3a displays the sensing electrical signals induced by applied compressive strain and detaching the three graphene pads from the P(VDF-TrFE) thin film one by one (from pad_1 to pad_3 in turn). A negative pulse voltage first emerged according to the enhanced piezopotential under compressive strain. Three positive pulse voltages were subsequently generated in sequence following the detachment orders due to the stepped hole extrication from the restriction of the electrostatic attractions. When the electrodes were released (from pad_3 to pad_1 in turn) and recovered to the initial state, three corresponding opposite voltages and a positive voltage emerged due to the flow back of accumulated charges. The output voltage values induced by detaching three graphene pads matched well with the voltages induced by releasing the detachments. The corresponding relationships of the sensing signals between detaching and releasing are important for the identification of multistage motions. In the case of subjection to tensile strain and stepped detachments (from pad_1 to pad_3), the output sensing signals are shown in Figure S6.

The laminated graphene electrodes on the pretailored top PDMS layer are also ready to be patterned into four columns (the top panel of Figure 3b). The electrode area of each patterned graphene column is 3 cm^2. When the multiple sensing columns were subjected to compressive strain and manipulated with detachments in turn (from column_1 to column_4), the corresponding sensing signals were observed in the bottom panel of Figure 3b. Compressive strain induced a negative pulse voltage, while the detachments induced four positive pulse voltages. Releasing the detachments and strains resulted in the flow back of the accumulated charges, representing opposite sensing signals. As shown in Figure S7, the laminated graphene electrodes were also patterned into two or three columns and tested under both tension and compression, respectively. The relevant output signals were observed according to different column numbers, promising the on-demand design capacity for different sensation requirements. As shown in Figure 3c, the four-column multiple sensing cell was attached in the palm to capture the motion of hand bending and fingers lifting. Four tailed graphene electrode columns were attached on the corresponding fingers. The output signals in Figure 3c were in agreement with the hand motions.

Moreover, the bottom PDMS substrate can be patterned with specific structures to increase the sensitivity of the NG sensing cell.[41−43] In this work, a rectangular groove structure was patterned on the bottom side of the PDMS substrate to enlarge the deformation space for applied strains (see Methods section). Figure 3d shows the cross-sectional diagram of the patterned device. The length (l) and height (h) of the groove pattern are 3 and 0.03 mm, respectively. The PDMS post length (l_p) is 24 mm. Generally, the aspect ratio (l/h) of the groove pattern is required to be smaller than 20 to escape from sagging. However, the length of the PDMS post in this work is much larger than the length of the groove pattern, excluding the collapse problem of the substrate. After patterning the groove, the NG sensor cell can efficiently detect the external pressures. When the external pressure was applied on the sensing cell, the deformation of the patterned grooves was equivalent to applying a compressive strain. As shown in Figure 3e, the output voltages of the patterned sensing cell increased from 0 to 0.8 V with the applied pressures increasing from 0 to 70 kPa (red curve). The output sensing signals showed a dramatic increment at pressure lower than 20 kPa and a mild increment at higher pressure over 20 kPa. However, the unpatterned sensing cell was unable to detect the applied pressure until the pressure was greater than 62.5 kPa to cause a deformation of the PDMS substrate. The output sensing voltages of patterned sensor were entirely higher than that of the unpatterned sensor due to the larger equivalent strains. When a pressure of 4 kPa was applied (Figure 3f), the patterned device had an output voltage of 0.1 V, while the unpatterned device nearly had no sensing signals. When the pressure was increased to 70 kPa (Figure S8a), the patterned sensor had an output voltage about 0.8 V, which was almost two times higher than the output sensing voltage of the unpatterned sensor. Furthermore, the patterned strain sensor can detect pressure less than 800 Pa, which belongs to low-pressure regime (Figure S8b). Patterning the groove in the PDMS substrate increases the sensitivity of pressure sensing without deteriorating the sensing ability of multistage sensation. The applied strain and detaching can also be detected, as shown in Figure S8c. To demonstrate a practical application of pressure sensing with the sensation matrix, an N-shaped acrylic plate was located on the matrix, and the corresponding contact positions were recorded (Figure S9a). According to the high flexibility of the PDMS substrate, P(VDF-TrFE) film, and graphene electrodes, the matrix was conformal to the human wrist and capable of distinguishing the touch points (Figure S9b).

Finally, the sensing performance of the sensation matrix (4 × 4 strain sensing cells) was characterized. Patterned graphene electrodes on the PDMS layers were laminated in a crisscross fashion. Each sensor cell had an area of 1 cm^2. Prior to the characterization of the sensation matrix, the electrical performance of each sensing pixel was tested under external compressive strains, as shown in Figure S10. All the sensor pixels operated well with stable output sensing voltages, which

DOI: 10.1021/acsnano.7b06126
ACS Nano XXXX, XXX, XXX−XXX

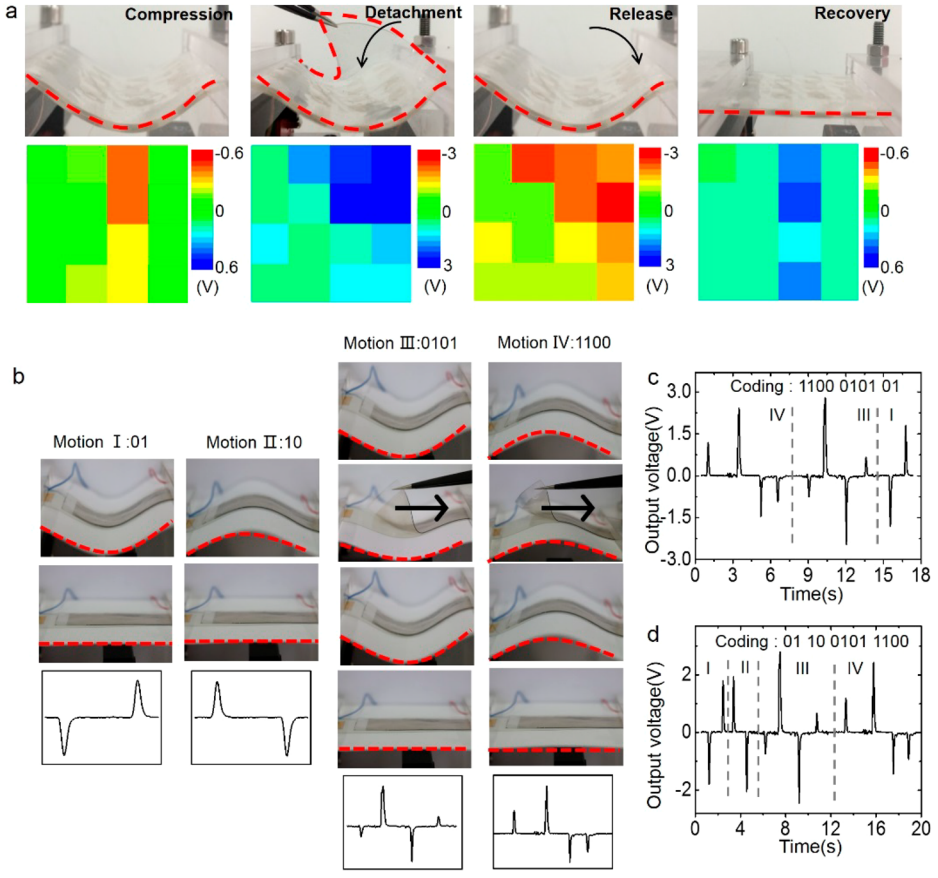

Figure 4. Sensing performance of the multistage sensation matrix and decoding application. (a) Top photographs show the motions (including compression, detachment, release, and recovery) applied to the sensation matrix. The bottom 2D color mappings represent the corresponding distributions of the corresponding sensing output voltages. (b) Definition of four basic motion combinations and the corresponding coding signals are shown at bottom. (c,d) Two series of induction signals decoded from the basic motion combinations.

was important for achieving accurate motion mapping. A combination of motions including compressing, detaching partial sensing cells, releasing the detachment, and recovering the strain was applied to the sensation matrix. The top photographs in Figure 4a show the motions of the sensation matrix. Two opposite edges of the matrix were fixed in a bending system. The output signal of each pixel in the matrix under different external motions was extracted. As shown in the bottom panel of Figure 4a, the 2D color mappings visually indicate the distributions of applied compressive strain/recovery and detachment/release with corresponding output sensing voltages, where the green color is set to be 0, blue is set to be positive, and red is set to be negative.

As the combination motions of compressive/tensile strains or detaching/releasing show individual output signals as discussed above, the proposed multistage sensors can work as a decoder to distinguish external complex motions. The positive output voltage is defined as "1", and the negative output voltage is defined as "0" according to the binary system. As shown in Figure 4b, four basic motion combinations are defined as "01", "10", "0101", and "1100", representing compression/recover (motion I), tension/recover (motion II), detaching/releasing at compression/recovery (motion III), and detaching/releasing at tension/recovery (motion IV). Afterward, we chose two groups of arbitrary encoded signals to test the corresponding decoding function. As shown in Figure 4c, the sensing signal is "1100 0101 01", which is concluded to be the combination of motion IV, III, and I depending on the matched signal values and directions. Based on the same criteria, the second signal is "01 10 0101 1100", which is conclude to be the combination of motion I, II, III, and IV.

CONCLUSION

In conclusion, we demonstrate a flexible and self-powered multistage sensation matrix based on transparent piezoelectric nanogenerator arrays with graphene as the electrodes. Each sensor cell in the matrix is capable of sequential multistage sensation to applied strain/recovery and detaching/releasing areas, which is a self-powering behavior without any external voltage inputs. With further structure engineering (such as tailoring into pads/columns or patterning with a groove structure), sophisticated multistage sensations and high sensitivity (minimum sensing pressure below 800 Pa) are achieved. Moreover, the sensation matrix is able to detect the distribution of strains and detaching areas in two-dimensional color mapping. According to the individual output signals, the sensing cell demonstrates decoding functions to distinguish external motion combinations. We believe this self-powered multistage sensation matrix is promising for a fully transparent and smart wearable E-skin system to detect complex motions with decoding capacities. Also, this research demonstrates one of the important applications of graphene as a robust flexible electrode for nanogenerators, which requires periodic mechanical triggering.

DOI: 10.1021/acsnano.7b06126
ACS Nano XXXX, XXX, XXX−XXX

METHODS

Material Preparation. The PDMS substrate was prepared by mixing the liquid PDMS elastomer (Sylgard 184, Dow Corning) and a curing agent in the ratio of 10:1 by weight. The liquid mixture was poured onto an acrylic plate, and then the sample was put into a chamber to remove bubbles in the PDMS layer by degassing. Finally, the PDMS substrate was peeled off from the acrylic plate after being cured in an oven at 70 °C for 1 h. Poly(vinylidene fluoride-*co*-trifluoroethylene) solution (20 wt %) was prepared by dissolving the P(VDF-TrFE) powder in *N*,*N*-dimethylformamide (DMF) solvent. The solution was stirred over 2 days to obtain a uniform solution. Large-area graphene was grown on a Cu foil (10 × 10 cm^2) through CVD following the method reported before.[36] The Cu foil was loaded into a quartz tube and annealed at 1000 °C under a H_2 atmosphere at low pressure for 1 h. Then, 5 sccm CH_4 was introduced for graphene growth under a continuous H_2 (10 sccm) flow. After 30 min, the CH_4 flow was ceased, and the tube was cooled to room temperature under the H_2 flow.

Device Fabrication. The graphene grown on the Cu foil was transferred onto the PDMS substrates (6 cm × 6 cm) through a standard wetting transfer method. Then the graphene was patterned by photolithography and subsequent RIE process as the bottom and laminated top electrodes on two PDMS substrates, respectively. After patterning, the as-prepared P(VDF-TrFE) solution was spin-coated onto one of the PDMS/graphene substrates (both terminals were protected by Kapton) at 2000 rpm for 40s, followed by drying at 60 °C for 10 min to remove the DMF solvent and subsequently annealed at 140 °C for 2 h in a N_2 atmosphere to enhance the piezoelectric β-phase of the P(VDF-TrFE). The Au pads were thermally deposited onto the terminals of each electrode for electrical wiring. Finally, the bottom PDMS layer and top PDMS layer were vertically laminated in a crisscross fashion to form a sensation matrix. The electrical poling process was carried out by applying an electric field of 5 MV/cm for 5 min between the top and bottom graphene electrodes (the thickness of the P(VDF-TrFE) film is 10 μm). Before the poling process, the dipolar moments in P(VDF-TrFE) film showed a random distribution of directions. After the poling process, the dipolar moments showed a preferential distribution toward the direction of the applied electric field. One time poling process is enough for long-term multistage sensation in this work. The groove-structure engineering on PDMS substrate was realized by casting PDMS liquid and curing agent onto a prepatterned SU-8 convex structure on Si wafer, which was prepared using standard photolithography techniques. The reverse reliefs were then replicated onto the bottom of PDMS substrate.

Device Measurements. The electrical properties of the strain sensor were measured using an oscilloscope (Tektronix TBS1104). The mechanical bending test was performed using a custom bending apparatus. The static pressures were applied onto the strain sensor through a numerical control force gauge comprising a steel pole terminated with a square-shaped silicon wafer plate (contact area = 2 cm^2), ranging from 0 to 2 N. The durability test was conducted with a linear motor. The morphology of the P(VDF-TrFE) film was measured by field-emission scanning electron microscopy (Hitachi SU8020). The crystallization of the P(VDF-TrFE) film was characterized by X-ray diffraction (X'Pert3 Powder). The transmittance was measured using a UV3600 spectrophotometer.

ASSOCIATED CONTENT

Supporting Information

The Supporting Information is available free of charge on the ACS Publications website at DOI: 10.1021/acsnano.7b06126.

Synchrotron XRD result and SEM image of the P(VDF-TrFE) film; UV−visible spectra of the strain sensor matrix; durability test and the output sensing signals after different bending cycles; definition of the bending strain; sensing electrical signals of the three-pad multistage sensor; output sensing signals of multiple-column sensors; sensing signals of the flexible multistage strain sensor with patterned and unpatterned substrate; electric sensing performance of the 4 × 4 sensor array (PDF)

AUTHOR INFORMATION

Corresponding Authors

*E-mail: sunqijun@binn.cas.cn.
*E-mail: zhong.wang@mse.gatech.edu.

ORCID

Jeong Ho Cho: 0000-0002-1030-9920
Qijun Sun: 0000-0003-2130-7389
Zhong Lin Wang: 0000-0002-5530-0380

Notes

The authors declare no competing financial interest.

ACKNOWLEDGMENTS

This work was supported by the National Key Research and Development Program of China (2016YFA0202703, 2016YFA0202704), the National Natural Science Foundation of China (51605034, 51711540300), the "Hundred Talents Program" of the Chinese Academy of Science, and the "Thousand Talents" program of China for pioneering researchers and innovative teams. Prof. J. H. Cho was supported by a grant from the Center for Advanced Soft Electronics (CASE) under the Global Frontier Research Program (2013M3A6A5073177).

REFERENCES

(1) Cai, L.; Song, L.; Luan, P.; Zhang, Q.; Zhang, N.; Gao, Q.; Zhao, D.; Zhang, X.; Tu, M.; Yang, F.; Zhou, W.; Fan, Q.; Luo, J.; Zhou, W.; Ajayan, P. M.; Xie, S. Super-Stretchable, Transparent Carbon Nanotube-Based Capacitive Strain Sensors for Human Motion Detection. *Sci. Rep.* **2013**, *3*, 3048.

(2) Chortos, A.; Bao, Z. Skin-Inspired Electronic Devices. *Mater. Today* **2014**, *17*, 321−331.

(3) Chortos, A.; Liu, J.; Bao, Z. Pursuing Prosthetic Electronic Skin. *Nat. Mater.* **2016**, *15*, 937−950.

(4) Hammock, M. L.; Chortos, A.; Tee, B. C. K.; Tok, J. B. H.; Bao, Z. 25th Anniversary Article: The Evolution of Electronic Skin (E-Skin): A Brief History, Design Considerations, and Recent Progress. *Adv. Mater.* **2013**, *25*, 5997−6037.

(5) Wang, X.; Dong, L.; Zhang, H.; Yu, R.; Pan, C.; Wang, Z. L. Recent Progress in Electronic Skin. *Adv. Sci.* **2015**, *2*, 1500169.

(6) Kim, D.-H.; Lu, N.; Ma, R.; Kim, Y.-S.; Kim, R.-H.; Wang, S.; Wu, J.; Won, S. M.; Tao, H.; Islam, A.; Yu, K. J.; Kim, T.-i.; Chowdhury, R.; Ying, M.; Xu, L.; Li, M.; Chung, H.-J.; Keum, H.; McCormick, M.; Liu, P.; Zhang, Y.-W.; Omenetto, F. G.; Huang, Y.; Coleman, T.; Rogers, J. A. Epidermal Electronics. *Science* **2011**, *333*, 838−843.

(7) Kim, J.; Lee, M.; Shim, H. J.; Ghaffari, R.; Cho, H. R.; Son, D.; Jung, Y. H.; Soh, M.; Choi, C.; Jung, S.; Chu, K.; Jeon, D.; Lee, S.-T.; Kim, J. H.; Choi, S. H.; Hyeon, T.; Kim, D.-H. Stretchable Silicon Nanoribbon Electronics for Skin Prosthesis. *Nat. Commun.* **2014**, *5*, 5747.

(8) Ho, D. H.; Sun, Q.; Kim, S. Y.; Han, J. T.; Kim, D. H.; Cho, J. H. Stretchable and Multimodal All Graphene Electronic Skin. *Adv. Mater.* **2016**, *28*, 2601−2608.

(9) Yamada, T.; Hayamizu, Y.; Yamamoto, Y.; Yomogida, Y.; Izadi-Najafabadi, A.; Futaba, D. N.; Hata, K. A Stretchable Carbon Nanotube Strain Sensor for Human-Motion Detection. *Nat. Nanotechnol.* **2011**, *6*, 296−301.

(10) Hwang, B.-U.; Lee, J.-H.; Trung, T. Q.; Roh, E.; Kim, D.-I.; Kim, S.-W.; Lee, N.-E. Transparent Stretchable Self-Powered Patchable Sensor Platform with Ultrasensitive Recognition of Human Activities. *ACS Nano* **2015**, *9*, 8801−8810.

DOI: 10.1021/acsnano.7b06126
ACS Nano XXXX, XXX, XXX−XXX

(11) Trung, T. Q.; Lee, N.-E. Flexible and Stretchable Physical Sensor Integrated Platforms for Wearable Human-Activity Monitoring and Personal Healthcare. *Adv. Mater.* **2016**, *28*, 4338−4372.
(12) Sun, Q.; Kim, D. H.; Park, S. S.; Lee, N. Y.; Zhang, Y.; Lee, J. H.; Cho, K.; Cho, J. H. Transparent, Low-Power Pressure Sensor Matrix Based on Coplanar-Gate Graphene Transistors. *Adv. Mater.* **2014**, *26*, 4735−4740.
(13) Ai, Y.; Lou, Z.; Chen, S.; Chen, D.; Wang, Z. M.; Jiang, K.; Shen, G. All rGO-on-PVDF-Nanofibers Based Self-Powered Electronic Skins. *Nano Energy* **2017**, *35*, 121−127.
(14) Kim, D.-H.; Xiao, J.; Song, J.; Huang, Y.; Rogers, J. A. Stretchable, Curvilinear Electronics Based on Inorganic Materials. *Adv. Mater.* **2010**, *22*, 2108−2124.
(15) Choi, S.; Lee, H.; Ghaffari, R.; Hyeon, T.; Kim, D.-H. Recent Advances in Flexible and Stretchable Bio-Electronic Devices Integrated with Nanomaterials. *Adv. Mater.* **2016**, *28*, 4203−4218.
(16) Sekitani, T.; Someya, T. Stretchable, Large-Area Organic Electronics. *Adv. Mater.* **2010**, *22*, 2228−2246.
(17) Ko, H. C.; Stoykovich, M. P.; Song, J.; Malyarchuk, V.; Choi, W. M.; Yu, C.-J.; Geddes, J. B., III; Xiao, J.; Wang, S.; Huang, Y.; Rogers, J. A. A Hemispherical Electronic Eye Camera Based on Compressible Silicon Optoelectronics. *Nature* **2008**, *454*, 748−753.
(18) Jeong, J.-W.; Yeo, W.-H.; Akhtar, A.; Norton, J. J. S.; Kwack, Y.-J.; Li, S.; Jung, S.-Y.; Su, Y.; Lee, W.; Xia, J.; Cheng, H.; Huang, Y.; Choi, W.-S.; Bretl, T.; Rogers, J. A. Materials and Optimized Designs for Human-Machine Interfaces *Via* Epidermal Electronics. *Adv. Mater.* **2013**, *25*, 6839−6846.
(19) Mannsfeld, S. C. B.; Tee, B. C. K.; Stoltenberg, R. M.; Chen, C. V. H. H.; Barman, S.; Muir, B. V. O.; Sokolov, A. N.; Reese, C.; Bao, Z. Highly Sensitive Flexible Pressure Sensors with Microstructured Rubber Dielectric Layers. *Nat. Mater.* **2010**, *9*, 859−864.
(20) Pan, L.; Chortos, A.; Yu, G.; Wang, Y.; Isaacson, S.; Allen, R.; Shi, Y.; Dauskardt, R.; Bao, Z. An Ultra-Sensitive Resistive Pressure Sensor Based on Hollow-Sphere Microstructure Induced Elasticity in Conducting Polymer Film. *Nat. Commun.* **2014**, *5*, 3002.
(21) Kim, S. Y.; Park, S.; Park, H. W.; Park, D. H.; Jeong, Y.; Kim, D. H. Highly Sensitive and Multimodal All-Carbon Skin Sensors Capable of Simultaneously Detecting Tactile and Biological Stimuli. *Adv. Mater.* **2015**, *27*, 4178−4185.
(22) Park, S.; Kim, H.; Vosgueritchian, M.; Cheon, S.; Kim, H.; Koo, J. H.; Kim, T. R.; Lee, S.; Schwartz, G.; Chang, H.; Bao, Z. Stretchable Energy-Harvesting Tactile Electronic Skin Capable of Differentiating Multiple Mechanical Stimuli Modes. *Adv. Mater.* **2014**, *26*, 7324−7332.
(23) Harada, S.; Kanao, K.; Yamamoto, Y.; Arie, T.; Akita, S.; Takei, K. Fully Printed Flexible Fingerprint-like Three-Axis Tactile and Slip Force and Temperature Sensors for Artificial Skin. *ACS Nano* **2014**, *8*, 12851−12857.
(24) Wang, Z. L.; Song, J. H. Piezoelectric Nanogenerators Based on Zinc Oxide Nanowire Arrays. *Science* **2006**, *312*, 242−246.
(25) Hu, Y.; Xu, C.; Zhang, Y.; Lin, L.; Snyder, R. L.; Wang, Z. L. A Nanogenerator for Energy Harvesting from a Rotating Tire and its Application as a Self-Powered Pressure/Speed Sensor. *Adv. Mater.* **2011**, *23*, 4068−4071.
(26) Hu, Y.; Wang, Z. L. Recent Progress in Piezoelectric Nanogenerators as a Sustainable Power Source in Self-Powered Systems and Active Sensors. *Nano Energy* **2015**, *14*, 3−14.
(27) Khan, U.; Kim, T.-H.; Lee, K. H.; Lee, J.-H.; Yoon, H.-J.; Bhatia, R.; Sameera, I.; Seung, W.; Ryu, H.; Falconi, C.; Kim, S.-W. Self-Powered Transparent Flexible Graphene Microheaters. *Nano Energy* **2015**, *17*, 356−365.
(28) Lee, S.; Bae, S.-H.; Lin, L.; Yang, Y.; Park, C.; Kim, S.-W.; Cha, S. N.; Kim, H.; Park, Y. J.; Wang, Z. L. Super-Flexible Nanogenerator for Energy Harvesting from Gentle Wind and as an Active Deformation Sensor. *Adv. Funct. Mater.* **2013**, *23*, 2445−2449.
(29) Lee, J.-H.; Lee, K. Y.; Kumar, B.; Tien, N. T.; Lee, N.-E.; Kim, S.-W. Highly Sensitive Stretchable Transparent Piezoelectric Nanogenerators. *Energy Environ. Sci.* **2013**, *6*, 169−175.
(30) Sun, Q.; Seung, W.; Kim, B. J.; Seo, S.; Kim, S.-W.; Cho, J. H. Active Matrix Electronic Skin Strain Sensor Based on Piezopotential-Powered Graphene Transistors. *Adv. Mater.* **2015**, *27*, 3411−3417.
(31) Zhang, L.; Xue, F.; Du, W.; Han, C.; Zhang, C.; Wang, Z. Transparent Paper-Based Triboelectric Nanogenerator as a Page Mark and Anti-Theft Sensor. *Nano Res.* **2014**, *7*, 1215−1223.
(32) Chu, H.; Jang, H.; Lee, Y.; Chae, Y.; Ahn, J.-H. Conformal, Graphene-Based Triboelectric Nanogenerator for Self-Powered Wearable Electronics. *Nano Energy* **2016**, *27*, 298−305.
(33) Ma, M.; Zhang, Z.; Liao, Q.; Yi, F.; Han, L.; Zhang, G.; Liu, S.; Liao, X.; Zhang, Y. Self-Powered Artificial Electronic Skin for High-Resolution Pressure Sensing. *Nano Energy* **2017**, *32*, 389−396.
(34) Bae, S.; Kim, H.; Lee, Y.; Xu, X.; Park, J.-S.; Zheng, Y.; Balakrishnan, J.; Lei, T.; Ri Kim, H.; Song, Y. I.; Kim, Y.-J.; Kim, K. S.; Ozyilmaz, B.; Ahn, J.-H.; Hong, B. H.; Iijima, S. Roll-to-Roll Production of 30-Inch Graphene Films for Transparent Rlectrodes. *Nat. Nanotechnol.* **2010**, *5*, 574−578.
(35) Lee, Y.; Bae, S.; Jang, H.; Jang, S.; Zhu, S.-E.; Sim, S. H.; Song, Y. I.; Hong, B. H.; Ahn, J.-H. Wafer-Scale Synthesis and Transfer of Graphene Films. *Nano Lett.* **2010**, *10*, 490−493.
(36) Li, X.; Magnuson, C. W.; Venugopal, A.; Tromp, R. M.; Hannon, J. B.; Vogel, E. M.; Colombo, L.; Ruoff, R. S. Large-Area Graphene Single Crystals Grown by Low-Pressure Chemical Vapor Deposition of Methane on Copper. *J. Am. Chem. Soc.* **2011**, *133*, 2816−2819.
(37) Li, M.; Wondergem, H. J.; Spijkman, M.-J.; Asadi, K.; Katsouras, I.; Blom, P. W. M.; de Leeuw, D. M. Revisiting the Delta-Phase of Poly(vinylidene fluoride) for Solution-Processed Ferroelectric Thin Films. *Nat. Mater.* **2013**, *12*, 433−438.
(38) Martins, P.; Lopes, A. C.; Lanceros-Mendez, S. Electroactive Phases of Poly(vinylidene fluoride): Determination, Processing and Applications. *Prog. Polym. Sci.* **2014**, *39*, 683−706.
(39) Zhou, T.; Zhang, L. M.; Xue, F.; Tang, W.; Zhang, C.; Wang, Z. L. Multilayered Electret Films Based Triboelectric Nanogenerator. *Nano Res.* **2016**, *9*, 1442−1451.
(40) Bae, S.-H.; Lee, Y.; Sharma, B. K.; Lee, H.-J.; Kim, J.-H.; Ahn, J.-H. Graphene-Based Transparent Strain Sensor. *Carbon* **2013**, *51*, 236−242.
(41) Xia, Y. N.; Whitesides, G. M. Soft Lithography. *Angew. Chem., Int. Ed.* **1998**, *37*, 550−575.
(42) Delamarche, E.; Schmid, H.; Michel, B.; Biebuyck, H. Stability of Molded Polydimethylsiloxane Microstructures. *Adv. Mater.* **1997**, *9* (9), 741−746.
(43) Qiu, X. Patterned Piezo-, Pyro-, and Ferroelectricity of Poled Polymer Electrets. *J. Appl. Phys.* **2010**, *108*, 011101.

DOI: 10.1021/acsnano.7b06126
ACS Nano XXXX, XXX, XXX−XXX